On the Importance of Hydrodynamic Interactions in Lipid Membrane Formation

Tadashi Ando and Jeffrey Skolnick*
Center for the Study of Systems Biology, School of Biology, Georgia Institute of Technology, Atlanta, Georgia

ABSTRACT Hydrodynamic interactions (HI) give rise to collective motions between molecules, which are known to be important in the dynamics of random coil polymers and colloids. However, their role in the biological self-assembly of many molecule systems has not been investigated. Here, using Brownian dynamics simulations, we evaluate the importance of HI on the kinetics of self-assembly of lipid membranes. One-thousand coarse-grained lipid molecules in periodic simulation boxes were allowed to assemble into stable bilayers in the presence and absence of intermolecular HI. Hydrodynamic interactions reduce the monomer-monomer association rate by 50%. In contrast, the rate of association of lipid clusters is much faster in the presence of intermolecular HI. In fact, with intermolecular HI, the membrane self-assembly rate is 3–10 times faster than that without intermolecular HI. We introduce an analytical model to describe the size dependence of the diffusive encounter rate of particle clusters, which can qualitatively explain our simulation results for the early stage of the membrane self-assembly process. These results clearly suggest that HI greatly affects the kinetics of self-assembly and that simulations without HI will significantly underestimate the kinetic parameters of such processes.

INTRODUCTION

Self-organization is one of the most fundamental phenomena in biology (1,2). Elucidating the mechanisms of the self-assembly of biological molecules, such as protein folding/binding (3,4), polymerization of cytoskeletal proteins (5), and the formation of lipid bilayer membranes (6), has been an important area of biological research for decades. For computational study, because these reactions take place on timescales of milliseconds to seconds, it is difficult if not impossible to simulate the entire self-assembly process by a conventional molecular-dynamics simulation of an atomistic protein-water system (7). Recently, a special-purpose parallel computer, ANTON, has opened the door to conducting millisecond-scale, atomistic, molecular-dynamics simulations for a relatively small system. In so doing, it has successfully captured protein folding and unfolding (8) as well as drug-binding events (9). Although this represents remarkable progress in computational biology, the employment of coarse-graining (where a reduced number of degrees of freedom is used to represent the simulated system (7,10,11)) is still necessary for large systems, such as intracellular environments and lipid membranes. Coarse-graining is not only useful for reducing computational cost but also for extracting the essential physical features from the simulations.

Brownian dynamics (BD) is one of the most important approaches to in silico experiments. BD has been used with coarse-grained (CG) models, where solvent molecules are not treated explicitly; rather, their dynamical effects on a solute molecule are incorporated in a stochastic manner consistent with hydrodynamics. An integration scheme for BD was developed by Ermak and McCammon in 1978 (12). The power of their BD algorithm is the ability to include hydrodynamic interactions (HI) through a position-dependent interparticle diffusion tensor. In addition, it is straightforward to compare simulations with and without HI in BD, which is an advantage over other hydrodynamic simulations such as lattice-Boltzmann approaches (13), multiparticle collision dynamics (14), and dissipative particle dynamics (15). If one is only interested in equilibrium thermodynamic properties, HI do not play any role and can be neglected.

However, HI can play a significant role in determining the dynamical properties of a given system (12). Theoretical studies showed that HI reduce the diffusion-controlled association of hard spheres by 46% with stick boundary conditions (16) and by 29% with slip boundary conditions (17). BD simulations demonstrated that the inclusion of HI between enzyme and ligands represented by spheres decreases their association rate by 20−30% (18). Recently, Frembgen-Kesner and Elcock (19) showed that HI between flexible model proteins also decrease their association rate by ~35−80%. Furthermore, the role of HI on protein folding has also been investigated. Baumketner and Hiwatari (20) found that HI delay folding of a β-hairpin but do not affect folding rates of an α-helical peptide. A speed-up of the folding of several proteins by 1.5−3-fold compared to simulations without HI has been reported (21,22). On the other hand, Kikuchi et al. (23) reported that HI accelerate polymer collapse, but that it has little effect on the folding kinetics of a model protein CI2. These studies clearly demonstrate the possible importance of HI

Submitted March 20, 2012, and accepted for publication November 26, 2012.

*Correspondence: skolnick@gatech.edu

Editor: Michael Feig.

0006-3495/13/01/0096/10 $2.00

http://dx.doi.org/10.1016/j.bpj.2012.11.3829

on the kinetics of protein-protein/ligand binding and protein folding.

Until now, while the effects of HI on the kinetics of association of pairs of molecules and protein folding have been examined, to our knowledge the effects of HI on the self-assembly of systems composed of many molecules has not been investigated. Thus, in this contribution, we investigate the possible role of HI in the self-assembly of biomolecules by conducting BD simulations of lipid membrane formation. Each lipid molecule is represented by two particles—a polar head and a hydrophobic tail. We also introduce a simple theoretical model to describe the effects of HI on the kinetics of self-assembly to provide a unified view of hydrodynamic effects. In the Discussion and then in the Conclusions, we examine the limitations and implications of our results for self-assembly processes in general.

METHODS

Brownian dynamics algorithm with HI

The integration algorithm for BD developed by Ermak and McCammon was used (12). For N Brownian particles, the propagation equation can be expressed as

$$\mathbf{r}(t+\Delta t) = \mathbf{r}(t) + \frac{\Delta t}{k_B T}\mathbf{D}\mathbf{F} + (\nabla \cdot \mathbf{D})\Delta t + \sqrt{2\Delta t}\mathbf{B}\mathbf{z}. \quad (1)$$

Here, $\mathbf{r}$ is the position vector of the N particles, t is the time, Δt is the time step, k_B is Boltzmann's constant, T is the temperature, $\mathbf{D}$ is the $3N \times 3N$ diffusion tensor, $\mathbf{F}$ is the $3N$-dimensional force vector determined by the gradient of potential energy, and $\mathbf{z}$ is the $3N$-dimensional Gaussian random noise vector, which has zero mean and variance of 1. $\mathbf{B}$ is a $3N \times 3N$ matrix that satisfies the following relationship:

$$\mathbf{D} = \mathbf{B}\mathbf{B}^T. \quad (2)$$

For a given $\mathbf{D}$, the matrix $\mathbf{B}$ is not unique. In our simulations, the Cholesky factorization method was used to obtain a lower-triangular matrix $\mathbf{B}$ (12). In this work, we employ the Rotne-Prager-Yamakawa (RPY) tensor for estimating $\mathbf{D}$ (24,25),

$$\mathbf{D}_{ij} = \begin{cases} \dfrac{k_B T}{6\pi\eta a}\mathbf{I} & i = j, \\ \dfrac{k_B T}{8\pi\eta r_{ij}}\left[\left(\mathbf{I} + \hat{\mathbf{r}}_{ij}\hat{\mathbf{r}}_{ij}\right) + \dfrac{2a^2}{r_{ij}^2}\left(\dfrac{1}{3}\mathbf{I} - \hat{\mathbf{r}}_{ij}\hat{\mathbf{r}}_{ij}\right)\right] & i \neq j \text{ and } r_{ij} \geq 2a, \\ \dfrac{k_B T}{6\pi\eta a}\left[\left(1 - \dfrac{9}{32}\dfrac{r_{ij}}{a}\right)\mathbf{I} + \dfrac{3}{32}\dfrac{r_{ij}}{a}\hat{\mathbf{r}}_{ij}\hat{\mathbf{r}}_{ij}\right] & i \neq j \text{ and } r_{ij} < 2a, \end{cases} \quad (3)$$

where a is the radius of particle, η is the viscosity of water, i and j are the indices of particles, $\mathbf{r}_{ij}$ is $\mathbf{r}_i - \mathbf{r}_j$, r_{ij} is the length of $\mathbf{r}_{ij}$, $\hat{\mathbf{r}}_{ij} = \mathbf{r}_{ij}/r_{ij}$, and $\mathbf{I}$ is the unit tensor. The RPY tensor has the property that $\nabla \cdot \mathbf{D} = 0$ so that the third term in Eq. 1 is dropped. For periodic boundary conditions, because the long-range contribution to HI is similar to electrostatic interactions, Ewald summation of the RPY tensor to obtain $\mathbf{D}$ is necessary not only for accuracy but also to ensure that $\mathbf{D}$ is positive-definite. We use the Ewald sum technique originally derived by Beenakker (26) and modified by Zhou and Chen (27) to allow for particle overlap.

Coarse-grained lipid model

Lipid molecules are represented by one head hydrophilic bead and one tail hydrophobic bead. A coarse-grained model lipid molecule is illustrated in Fig. S1 in the Supporting Material. The Stokes radii of the beads are assigned as 6.5 Å. These beads are connected by a harmonic potential,

$$V_{ij}^{\text{bond}} = \frac{1}{2}k^{\text{bond}}\left(r_{ij} - r_0\right)^2, \quad (4)$$

where k^{bond} is the force constant, r_{ij} is the distance between head and tail beads in a given molecule, and r_0 is the equilibrium bond length between head and tail beads. In our simulations, $k^{\text{bond}} = 1000\ k_B T/r_0^2$ and $r_0 = 13$ Å were used. Nonbonded interactions between molecules consist of repulsive and attractive terms. Repulsive interactions are described by a half-harmonic potential

$$V_{ij}^{\text{rep}} = \begin{cases} \dfrac{1}{2}k^{\text{rep}}\left(r_{ij} - r_{c,ij}\right)^2 & r_{ij} \leq r_{c,ij}, \\ 0 & r_{ij} > r_{c,ij}. \end{cases} \quad (5)$$

Here, k^{rep} is the force constant of 10 $k_B T/\text{Å}^2$, r_{ij} is the distance between beads i and j, and $r_{c,ij}$ is the contact distance for beads i and j. For an effective cylindrical lipid shape, we used $r_{c,\text{ head-head}} = 11.7$ Å, $r_{c,\text{ head-tail}} = 12.35$ Å, and $r_{c,\text{ tail-tail}} = 13.0$ Å. The attractive part that is only operative between tail-tail beads pair is described by a function introduced by Cooke et al. (28),

$$V_{ij}^{\text{attr}} = \begin{cases} -\varepsilon_L & r_{ij} \leq r_{c,ij}, \\ -\varepsilon_L \cos^2\left(\dfrac{\pi\left(r_{ij} - r_{c,ij}\right)}{2w_c}\right) & r_{c,ij} < r_{ij} \leq r_{c,ij} + w_c, \\ 0 & r_{ij} > r_{c,ij} + w_c. \end{cases} \quad (6)$$

This gives an attractive potential with a depth of ε_L, in which the energy smoothly decays to zero for $r_{c,ij} < r_{ij} < r_{c,ij} + w_c$. The values ε_L and w_c are key parameters in this model. In our model, $\varepsilon_L = 1.9\ k_B T$ and $w_c = 19.5$ Å ($w_c/r_{c,\text{ tail-tail}} = 1.5$).

Simulation conditions

To study the effects of HI on the self-assembly of the CG lipid model, we performed two different types of BD simulations: one with full HI (in which hydrodynamic interactions within each lipid molecule as well as between lipid molecules are considered), and the other is a simulation

with intramolecular HI only (in which intermolecular hydrodynamic interactions are neglected). Hereafter, we call the former "with inter-HI" and the latter "without inter-HI". The differences in simulation results between the two conditions reflect the effect of intermolecular HI. It is well known that neglecting HI within a polymer significantly slows down its diffusion constant (29,30). In BD simulations with HI and without HI, the diffusion coefficients of monomer molecules at infinite dilution obtained from these simulations would be significantly different. Therefore, we did not perform simulations without intramolecular-HI.

For BD simulations, 1000 CG lipid molecules were randomly placed in a $28 \times 28 \times 28$ nm^3 periodic box without significant overlap between particles. For each condition, 50 independent initial configurations were generated. The time step was 0.56 ps, which corresponds to $0.5 \times 10^{-3}\ a^2/D_0$, with $D_0 = k_BT/6\pi\eta a$. Simulations with and without inter-HI were performed for 4 μs and 8 μs, respectively. The diffusion tensor and its decomposition were updated every 50 steps. The simulation temperature was set to 298 K.

Analysis

To measure lipid-membrane ordering, we evaluated the nematic order parameter S of the system, which is given by the largest eigenvalue of an order parameter defined by a 3×3 matrix (31) as

$$Q_{\alpha\beta} = \frac{1}{2}\langle 3\cos\theta_\alpha \cos\theta_\beta - \delta_{\alpha\beta}\rangle \ \text{ with } \ \alpha,\beta \in \{x,y,z\}. \quad (7)$$

Here, θ_α is the angle between the lipid molecule axis and the α-axis, $\delta_{\alpha\beta}$ is the Krönecker delta function, and the angle brackets represent the average over all molecules in the system. The eigenvector corresponding to the eigenvalue S is the bilayer norm. S equals 1 for perfectly aligned molecules and 0 for a random configuration.

Clustering of lipid molecules was performed based on the following criterion: If the distance between the tail particles of a given lipid pair is <15 Å, they are part of a given cluster.

Translational diffusion coefficients in dilute solutions of various-size lipid clusters were estimated from BD simulations with free-boundary conditions. The translational diffusion coefficients, D, were estimated by

$$6D\tau = \left\langle \left(\mathbf{x}_{\rm cm}(t+\tau) - \mathbf{x}_{\rm cm}(t)\right)^2 \right\rangle, \quad (8)$$

where $\mathbf{x}_{\rm cm}(t)$ is the center-of-mass position vector of the lipid cluster at time t, and the angle brackets indicate an average over configurations separated by a time difference τ.

For estimating the in-plane translational diffusion coefficient of lipids, $D_{\rm b}$, the following equation was used:

$$4D_{\rm b}\tau = \left\langle \left(\mathbf{x}_{||}(t+\tau) - \mathbf{x}_{||}(t)\right)^2 \right\rangle, \quad (9)$$

where $\mathbf{x}_{||}(t)$ is the projection of center-of-mass position vector of the lipid at time t into the bilayer plane. Those lipids that diffused away from average bilayer plane by >50 Å were eliminated from the averaging in Eq. 9.

To analyze the correlations between lipids in time and space, we calculated the normalized pair correlation function, C_{ij}, given by

$$C_{ij}(d_0,\tau) = \frac{\sum\left[\left(\Delta\mathbf{x}_i(\tau)\cdot\Delta\mathbf{x}_j(\tau)\right)\delta\left(d_0 - d_{ij}\right)\right]}{\sqrt{\sum\left|\Delta\mathbf{x}_i(\tau)\delta\left(d_0 - d_{ij}\right)\right|^2}\sqrt{\sum\left|\Delta\mathbf{x}_j(\tau)\delta\left(d_0 - d_{ij}\right)\right|^2}}, \quad (10)$$

where $\Delta\mathbf{x}_i(\tau)$ is the displacement of center-of-mass of lipid molecule i between the time t and $t+\tau$, d_0 is a specified distance between tail particles of lipids i and j, d_{ij} is the distance between tail particles of lipids i and j at time t, and $\delta(d_0 - d_{ij})$ is the Dirac delta function. The summation in Eq. 10 is over all time points t and all lipid pairs. The value C_{ij} ranges from -1 to 1. When two particles are positively correlated, C_{ij} assumes a positive value, and when negatively correlated, C_{ij} is negative.

RESULTS

Self-assembly into a stable bilayer and its kinetics

We would expect that the lipid molecules form a well-defined lipid bilayer in the simulation box. To validate our CG lipid model, we carried out self-assembly simulations of 1000 CG lipid molecules, starting from random configurations in a $28 \times 28 \times 28$ nm^3 periodic box. This corresponds to a particle density of 9.0×10^{-2} particles/nm^3 and a volume fraction of 0.1. Fifty independent simulations were performed both with and without inter-HI. The degree of alignment of lipid molecules can be quantified by the nematic order parameter S defined in Eq. 7. Representative trajectories of the time evolution of S in the simulations with and without inter-HI are shown in Fig. 1, in which an S value of 0.7 corresponds to well-defined, stable bilayers spanning the entire simulation box (see Fig. 2 *D*). In some of the trajectories, S stays in the range of 0.5–0.6 for a certain period of time. This state corresponds to the well-defined lipid bilayers, which do not span the entire box (see Fig. 2 *E*). Most of the lipid molecules make lipid bilayers, but further global rotation of the lipid bilayer plane is necessary to form a complete membrane in the simulation box. Without periodic boundary conditions, these states would not be observed. Therefore, hereafter, we call this state a "pseudo-intermediate".

Based on this observation, we classify trajectories into four different groups: For Group A, S values reach 0.7 without traversing the pseudo-intermediate states. For Group B, the simulation systems stay in the pseudo-intermediate states for >0.5 μs, and then the edges of the bilayers are merged to form box-spanning bilayers, in which the residence time for the intermediate state is measured as follows: The average S value for the intermediate state, $\langle S_{\rm inter}\rangle$, is calculated over a manually defined time period for each trajectory and then the time period between the time points when the system reach $S > \langle S_{\rm inter}\rangle$ and $S > 0.7$ is calculated. For Group C, the systems reach the pseudo-intermediate states, but complete box-spanning lipid bilayers are not observed within the given simulation time. For Group D, S values fluctuate under 0.5 over the course of the entire simulation. In Table 1, the numbers of trajectories for

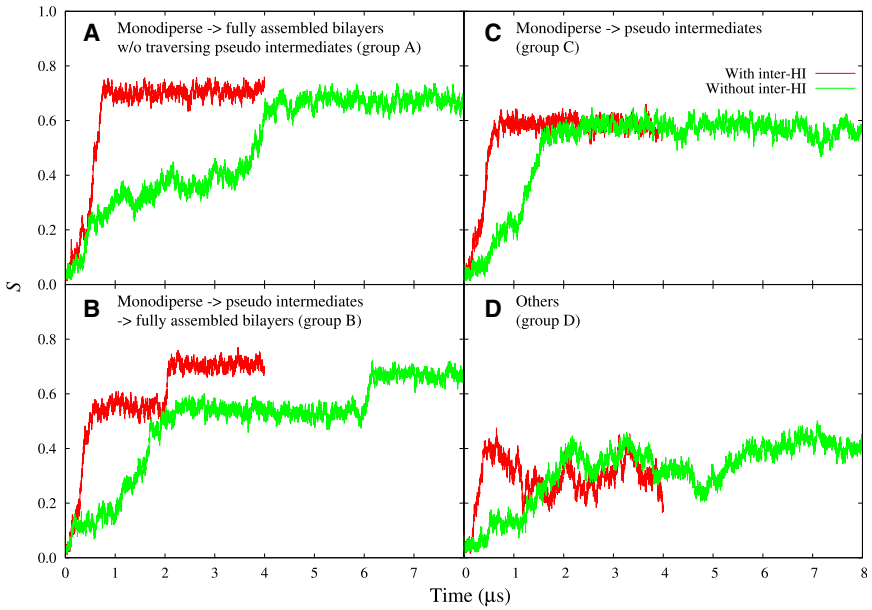

FIGURE 1 Representative trajectories of nematic order parameter S as a function of simulation time for BD simulations in the presence and absence of inter-HI for four different types. (*A*) Group A. (*B*) Group B. (*C*) Group C. (*D*) Group D.

each group in the presence and absence of inter-HI are listed. In 29 of 50 simulations with inter-HI and 17 of 50 simulations without inter-HI, S values reached 0.7 within 4-μs and 8-μs simulation times, respectively.

Snapshots of the self-assembly process are shown in Fig. 2. Movies are also provided in the Supporting Material.

For all trajectory groups, by ~0.2 μs, the lipid monomers that were initially randomly placed in the box quickly aggregate into a number of small clusters or micelles. After that, they fuse into a large leaflet-like cluster along a certain direction in the periodic box. For Group A, the cluster zips up to form a bilayer spanning the whole periodic box

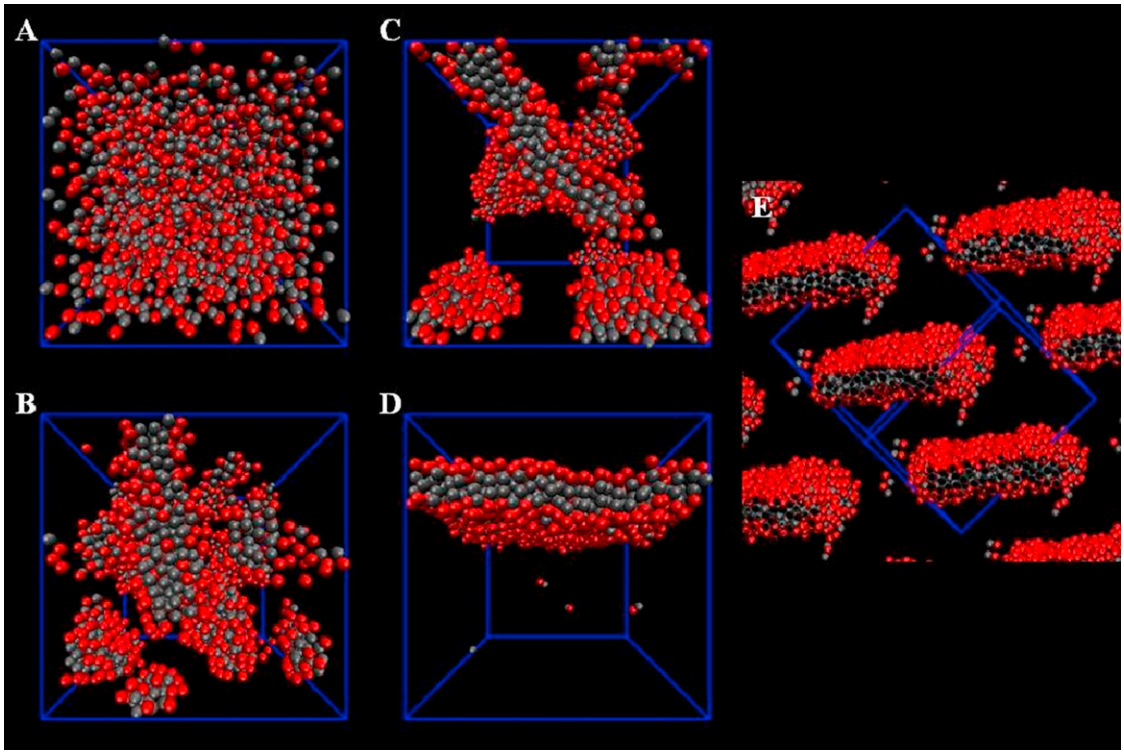

FIGURE 2 Snapshots of lipid self-assembly pathways. Configurations of the simulation in the presence of inter-HI presented in Fig. 1 *A* (*A*) at time 0 μs, (*B*) at 0.1 μs, (*C*) at 0.3 μs, and (*D*) at 1 μs. S values for these states are 0.09, 0.08, 0.19, and 0.71, respectively. Configuration of the pseudo-intermediate state observed in the simulation with inter-HI presented in Fig. 1 *B* at 1 μs is shown in (*E*). In panel *E*, lipid molecules in the first neighbor cells are also shown. This figure was generated by VMD (43).

TABLE 1 Numbers of trajectories for the four different trajectory types observed in the BD simulation with inter-HI for 4 μs and without inter-HI for 8 μs

Group	Trajectory description	With inter-HI	Without inter-HI
A	Fully box-spanning lipid bilayers are formed without traversing pseudo-intermediates	17	12
B	Fully box-spanning lipid bilayers are formed via pseudo-intermediates	12	5
C	Pseudo-intermediates are formed, but fully box-spanning lipid bilayers are not formed	16	29
D	Others	5	4

without going through pseudo-intermediate states. For Groups B and C, the cluster makes a flat membrane spanning a certain direction in the box, and is trapped in a pseudo-intermediate state. Then, for Group B, the edges of the membrane are merged via a global rotation of the membrane, which is a very slow process. For Group D, most lipid molecules are assembled into a large cluster, but they do not form flat membrane bilayers. These pathways are the same in BD simulations with and without inter-HI.

To quantify the HI effects on kinetics of membrane self-assembly, we estimate the rate constants k and mean first passage time (MFPT) of these self-assemblies (Fig. 3). The time evolution of the fraction of trajectories that reach $S > 0.7$ for all groups could be fit by first-order kinetics, from which we deduce that $k = 0.23\ \mu s^{-1}$ and $0.05\ \mu s^{-1}$, with and without inter-HI simulations, respectively (Fig. 3 *A*). Thus, inter-HI accelerate the overall rate of self-assembly of CG lipid molecules by 4.6-fold compared to a BD simulation without inter-HI. As we mentioned above, the intermediate states observed in the simulations could be an artifact introduced by the periodic boundary condition. Therefore, we evaluate the kinetics of membrane self-assembly only for Group A in Fig. 3 *B*. The MFPTs of membrane self-assembly in the presence and absence of inter-HI are 1.1 μs and 3.3 μs, respectively, showing a threefold acceleration of assembly process by inter-HI. In Fig. 3, *C* and *D*, the kinetics of membrane self-assembly process for Groups B and C are shown.

When the membrane self-assembly processes proceed via pseudo-intermediate states, inter-HI increase the rate by 10-fold (Fig. 3 *C*). For these groups, the MFPT from the initial configurations to the pseudo-intermediate states, that is, the time required for $S > \langle S_{\text{inter}} \rangle$ from 0 μs, was 0.68 μs in the presence of inter-HI and was 1.64 μs in the absence of inter-HI (data not shown). The rate constants for formation from the pseudo-intermediate states to the fully assembled, box-spanning membrane for Groups B and C are estimated to be 0.16 μs^{-1} and 0.02 μs^{-1} in the simulations with and without inter-HI, respectively (Fig. 3 *D*). These results consistently suggest that inter-HI could accelerate membrane self-assembly processes. Of particular note is that inter-HI could play an important role in the global motions, as seen in Fig. 3 *D*.

In Fig. 4 *A*, the growth of average lipid-cluster size averaged over 50 simulations up to 0.1 μs and their slopes around an average cluster size $\langle N_{\text{lipid}} \rangle$ of 1 and 10 are shown. At 0.1 μs, the maximum cluster sizes averaged over 50 simulations with and without inter-HI were ~340 and ~230, respectively, suggesting that many lipid clusters or micelles are present on this timescale. The ratios of the slopes of the growth curves in the simulation in the presence and absence of inter-HI, g(with inter-HI)/g(without inter-HI), at various average cluster sizes are shown in Fig. 4 *B*.

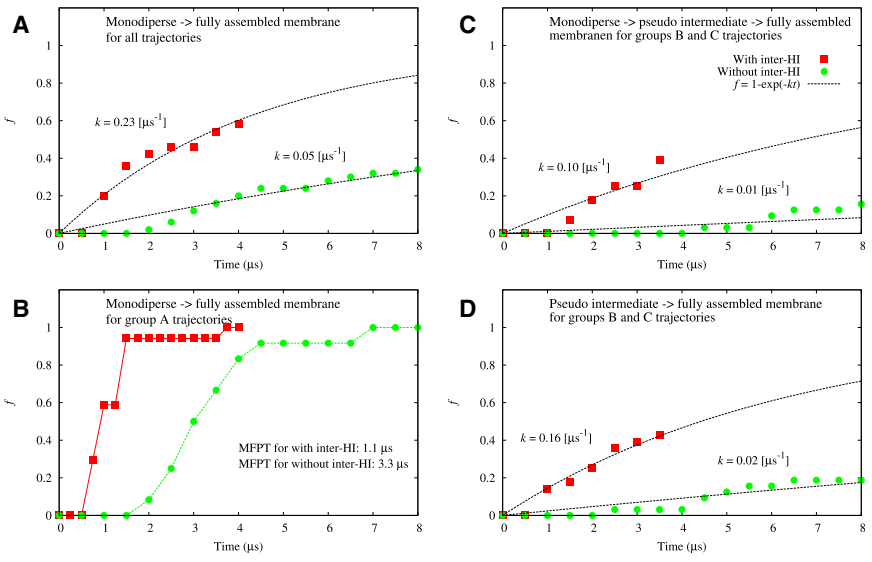

FIGURE 3 Kinetics of membrane self-assembly in the presence of inter-HI and in the absence of inter-HI. (*A*) The fraction systems that reached $S > 0.7$ for all trajectories within the given time period from 0 μs. (*B*) The fraction systems that reached $S > 0.7$ for trajectories in Group A within the given time period from 0 μs. Mean first passage times (MFPT) are also shown. (*C*) The fraction systems that reached $S > 0.7$ for trajectories in Groups B and C within the given time period from 0 μs. (*D*) The fraction systems that reach $S > 0.7$ from the intermediate states for trajectories in Groups B and C within the given time period from time points when the systems reached intermediate states. The value f is the fraction of systems that satisfied given criteria. (*Black dotted lines*) Fit to the date with 1–exp($-kt$), where k is the apparent kinetic parameter and t is the time. Values of k are also shown in panels *A*, *C*, and *D*.

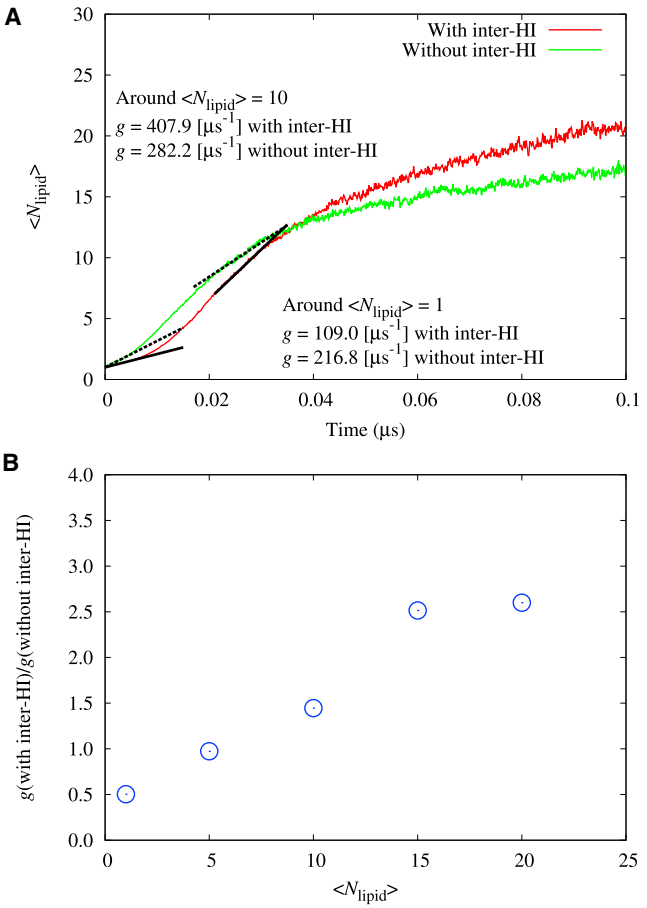

FIGURE 4 (*A*) Growth of average lipid-cluster sizes $\langle N_{\text{lipid}}\rangle$ up to 0.1 μs $\langle N_{\text{lipid}}\rangle$ is averaged over 50 simulations. (*B*) The ratios of the slopes of the growth curves in the simulation in the presence and absence of inter-HI g(with inter-HI)/g(without inter-HI) for various $\langle N_{\text{lipid}}\rangle$. For estimating the slopes, the following time ranges were used: In the simulation with inter-HI, 0–4 ns for $\langle N_{\text{lipid}}\rangle = 1$; 12–19 ns for $\langle N_{\text{lipid}}\rangle = 5$; 26–30 ns for $\langle N_{\text{lipid}}\rangle = 10$; 40–60 ns for $\langle N_{\text{lipid}}\rangle = 15$; and 70–120 ns for $\langle N_{\text{lipid}}\rangle = 20$. For simulations without inter-HI, 0–4 ns for $\langle N_{\text{lipid}}\rangle = 1$, 10–17 ns for $\langle N_{\text{lipid}}\rangle = 5$; 22–28 ns for $\langle N_{\text{lipid}}\rangle = 10$; 50–80 ns for $\langle N_{\text{lipid}}\rangle = 15$; and 120–280 ns for $\langle N_{\text{lipid}}\rangle = 20$. The slopes at $\langle N_{\text{lipid}}\rangle = 1$ and 10 for simulations with (*solid lines*) and without HI (*dotted lines*) are shown as examples in panel *A*.

At $\langle N_{\text{lipid}}\rangle = 1$, where monomer-monomer associations dominate, g(with inter-HI)/g(without inter-HI) = 0.50. This result indicates that inter-HI decelerate monomer-monomer association. However, this ratio increases with average cluster size, and for $\langle N_{\text{lipid}}\rangle > 5$, inter-HI accelerate the association rates. These results clearly indicate that the effect of inter-HI depends on the size of the lipid cluster and that the relative acceleration of association kinetics increases with increasing lipid-cluster size.

Physical mechanisms of the hydrodynamic interaction effects on self-assembly processes

The results of two sets of BD simulations clearly show that intermolecular HI have a striking effect on lipid membrane assembly kinetics. What is the physical origin of this effect? To address this question, we will introduce a simple theory that explains the cluster-size dependence of diffusive encounter rate. We also show correlated motions between lipid molecules induced by HI.

Theory for diffusion-controlled kinetics

Many of bimolecular reactions in solution are limited by the rate of diffusive encounter between reactive species. The effect of HI on the diffusion-controlled rate coefficient for spherical particles has been studied theoretically (16). The rate of diffusive encounter, k_{D}, can be described by (32)

$$k_{\text{D}} = 4\pi\left[\int_{\sigma}^{\infty}\frac{\exp\left[\frac{W(r)}{k_{\text{B}}T}\right]}{D(r)r^2}dr\right]^{-1}, \tag{11}$$

where $W(r)$ is the potential mean force between the reactants at center-to-center distance r, σ is the encounter distance, and $D(r)$ is the distance-dependent relative translational diffusion coefficient. When each reactant is represented by a sphere, $D(r)$ in dilute conditions can be written by

$$D(r) = D_1 + D_2 - 2\hat{\mathbf{r}}_{12}\cdot\mathbf{D}_{12}\cdot\hat{\mathbf{r}}_{12}. \tag{12}$$

Here, $\mathbf{D}_{12}$ is diffusion tensor between particles 1 and 2; $\hat{\mathbf{r}}_{12}$ is the unit vector between reactants; and D_i is the diffusion coefficient of particle i for stick boundary conditions, and is given by

$$D_i = \frac{k_{\text{B}}T}{6\pi\eta a_i}, \tag{13}$$

where a_i is the radius of particle i. Let us assume $W(r) = 0$. In the absence of HI that is the free-draining (FD) limit, because $\mathbf{D}_{12} = 0$, the relative diffusion coefficient is a constant and is the sum of the diffusion coefficients of the reactants. Therefore,

$$k_{\text{D}}^{\text{FD}} = 4\pi(D_1 + D_2)\sigma. \tag{14}$$

This is the Smoluchowski expression (33). In the presence of HI at the Oseen tensor level for stick boundary conditions (34), $D(r)$ is given by

$$D(r) = D_1 + D_2 - \frac{k_{\text{B}}T}{2\pi\eta r_{12}}. \tag{15}$$

Then, the encounter rate is expressed as

$$k_{\text{D}}^{\text{Oseen}} = \frac{2k_{\text{B}}T}{\eta}\left[\ln\frac{(D_1+D_2)\sigma}{(D_1+D_2)\sigma - \frac{k_{\text{B}}T}{2\pi\eta}}\right]^{-1}, \tag{16}$$

where σ is the distance to react. When the reactants have the same radius, then $a_1 = a_2 = a_0$, and $\sigma = 2\,a_0$, Eqs. 14 and 16 reduce to

$$k_D^{FD} = 16\pi D_0 a_0 \tag{17}$$

and

$$k_D^{Oseen} = \frac{12\pi D_0 a_0}{\ln 4} \tag{18}$$

with

$$D_0 = \frac{k_B T}{6\pi\eta a_0}. \tag{19}$$

When the reactants are represented by single particles having the same radius, the diffusive encounter rate is independent of radius for both FD and Oseen, and its ratio $k_D{}^{Oseen}/k_D{}^{FD}$ is 0.54. This theoretical analysis was originally done by Deutch and Felderhof (16). This theory shows that hydrodynamic interactions reduce the relative diffusion coefficient of reactants as in Eq. 15, resulting in the reduction of the diffusive encounter rate between them.

Next, we combine Deutch-Felderhof theory with the Rouse/Zimm model that describes diffusion of random polymer chains (30,35,36). The diffusion coefficient of a random polymer connecting N identical beads with radius a in the presence of HI shows the following scaling property:

$$D^{Oseen} \approx D_0 N^{-\nu} \quad (0<\nu<1). \tag{20}$$

Here, D^{Oseen} is the diffusion coefficient of the polymer. The hydrodynamic radius of the polymer a is related to its diffusivity D^{Oseen} by

$$a = \frac{k_B T}{6\pi\eta D^{Oseen}}. \tag{21}$$

Thus, the radius of polymer has N^{ν} scaling. Because D_0 and a_0 in Eq. 18 can be replaced with D^{Oseen} and a, respectively, the diffusive encounter rate in the presence of HI does not show an N dependence for the reactant pair consisting of the same number of beads. That is,

$$k_D^{Oseen} = \frac{12\pi D^{Oseen} a}{\ln 4} = \frac{2k_B T}{\eta \ln 4}. \tag{22}$$

In the FD limit, the diffusion coefficient D^{FD} is given by

$$D^{FD} \approx D_0 N^{-1}. \tag{23}$$

Because HI only affects kinetics and not thermodynamics, polymers have the same radius in the presence and absence of HI, which scales with N^{ν} (see Eqs. 20 and 21). Using Eqs. 17, 20, 21, and 23, we obtain the following scaling properties for the encounter rate in the FD limit:

$$k_D^{FD} = 16\pi D^{FD} a = \frac{8k_B T}{3\eta} N^{\nu-1}. \tag{24}$$

The ratio of the diffusive encounter rate $k_D{}^{Oseen}/k_D{}^{FD}$ is proportional to the ratio of diffusion coefficients D^{Oseen}/D^{FD}, which is given by

$$\frac{k_D^{Oseen}}{k_D^{FD}} = \frac{3}{4\ln 4}\frac{D^{Oseen}}{D^{FD}} \approx 0.54\,N^{1-\nu}. \tag{25}$$

For the diffusion-limited encounter rate with the RPY tensor $k_D{}^{RPY}$, an analytical solution of Eq. 11 may not be obtained. However, at long distances, the Oseen tensor well represents the RPY tensor. Using this property, we numerically integrated Eq. 11 with the RPY tensor for the short-range part and the equation with the Oseen tensor was analytically solved as shown above for a long-range part. This gives

$$\frac{k_D^{RPY}}{k_D^{FD}} \approx 0.60\,N^{1-\nu}. \tag{26}$$

The ratio for the reactant pair consisting of different bead numbers is described in the Supporting Material. In poor solvents where the polymer collapses into a compact conformation, ν is predicted to be ~1/3 (29). Equations 25 and 26 with ν of 1/3 predict that for N smaller than 3, the diffusive encounter rate in the absence of HI is faster than that in the presence of HI, and that once N is larger than 3, this trend is reversed.

In order to check applicability of this simple theory to the lipid association process, we estimated diffusive encounter rates, using the Northrup-Allison-McCammon method (37), from a series of BD simulations of small lipid-cluster pairs in the presence and absence of inter-HI. These values were in good agreement with the theory when each lipid molecule is treated as a single sphere. Details of this comparison are discussed in the Supporting Material.

The theory suggests the following conclusions: The ratio of the diffusive encounter rate in the presence and absence of HI is proportional to the ratio of diffusion coefficients in these conditions. For a reactant pair consisting of the same number of beads, the diffusion encounter rate in the presence of HI is constant. On the other hand, in the absence of HI, the diffusive encounter rate decreases as a function of N. Therefore, comparing simulation results of diffusive association models in the absence and presence of hydrodynamic interactions, HI accelerates the association rates compared to FD simulations, and HI is a more important role for larger N.

It is important to note the difference in units of the slopes of the lipid-cluster growth g estimated from BD simulation results, and the diffusive encounter rates k_D in

the theory: the former has the units of s^{-1} and the latter has units of mol^{-1} m^3 s^{-1}. In the former, we are comparing the time dependence of the number of molecules in a given lipid cluster. In the latter, we are comparing the rate of diffusion encounter of a pair of identical size lipid clusters that fuse to a larger cluster. The initial slope of g(with inter-HI)/g(without inter-HI) is 0.50, which is in reasonable agreement with the analytical result $k_D^{RPY}/k_D^{FD} = 0.60$ for $N = 1$ in Eq. 26. As assembly proceeds, growth happens not only when a pair of identical size lipid-clusters fuse; instead, the lipid grows by the coalescence of heterogeneous size lipid-clusters (see Fig. S2). Nevertheless, the trend of increase of g(with inter-HI)/g(without inter-HI) with $\langle N_{lipid} \rangle$ observed in BD simulation results is qualitatively consistent with the analytical model described in Eqs. 25 and 26. We believe that our theoretical model can capture an essence of HI effects on membrane self-assembly.

Correlated motions between lipids

Once lipids form a large cluster, zipping-up is the next step to form stable bilayers spanning the periodic box. The theory described above could explain the effects of HI on the diffusion-controlled kinetics for pairs of lipid clusters. However, the model may not be appropriate for explaining the zipping-up of partially organized lipid membranes, because this process is dominated by the internal motions of the membrane. To investigate differences of motions of the lipid between two conditions, in-plane diffusion coefficients of lipids, D_b, and the dynamical correlations in time and space between lipids were examined using the trajectories after formation of stable bilayers. If significant correlated motions exist, the zipping-up would be accelerated. Actually, transitions from the pseudo-intermediate states to the box-spanning lipid bilayers in the presence of inter-HI are 10 times faster than those in the absence of inter-HI, as shown in Fig. 3 *D*. For in-plane diffusion, significant differences in D_b are not observed; $D_b = 33.5$ $nm^2/\mu s$ and 31.6 $nm^2/\mu s$ in simulations with and without inter-HI, respectively (see Fig. S5). Although these values are ~3 times larger than a typical value for the lateral diffusion coefficient of lipid in phospholipid bilayer membranes, namely 10 $nm^2/\mu s$ (38), they are in reasonable agreement when considering that a schematic CG model is used.

Normalized pair correlation functions, C_{ij}, of lipid pairs for BD simulations with and without inter-HI are shown in Fig. 5, in which C_{ij} ranges from -1 to 1 and $C_{ij} > 0$ for positively correlated lipid pairs and $C_{ij} < 0$ for negatively correlated lipid pairs. In the simulation without inter-HI, for lipid pairs in a monolayer, $C_{ij} < 0.2$ even at short time and distances. In contrast, for pairs in the same and opposing monolayers, a significant positive intermolecular dynamic correlation in the simulations with inter-HI is evident which is operative over a distance of 40 Å (corresponding to the third lipid solvation shell) and for 0.5 μs. These results suggest that the correlated motions between lipids in the membrane caused by inter-HI accelerate the zipping-up motions of lipid membranes in the late stages of the lipid membrane self-assembly processes.

DISCUSSION

The main goal of this study is to evaluate the possible role of HI in the self-assembly of biological molecules. Toward this purpose, we simulated the formation of lipid bilayers by BD in the presence and absence of inter-HI, in which each lipid is represented by two spheres and 1000 lipid molecules are in the periodic box. We also introduced a simple theory that approximately describes the size dependence of hydrodynamic effects on the diffusive encounter rate of a reactive object pair. Our simulations show that inter-HI accelerate the overall rate of membrane self-assembly by 3- to

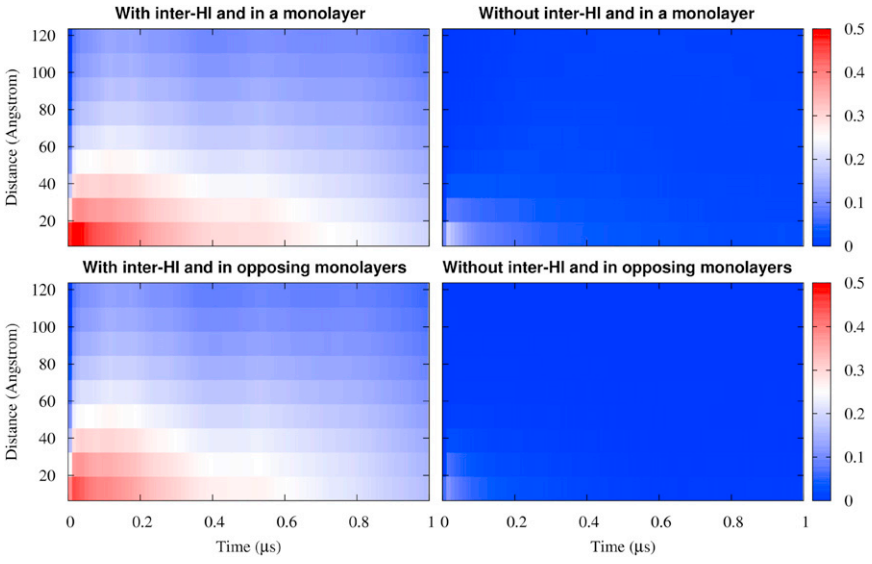

FIGURE 5 Normalized pair correlation function, C_{ij}, between lipids.

10-fold. Therefore, HI play a more important role in the kinetics of membrane assembly than in protein folding.

In the beginning of the assembly process, monomer-monomer association dominates. Deutch-Felderhof theory predicts a 46% reduction in the diffusive association rate of a hard-sphere pair. This reduction is caused by the fact that intermolecular HI create positively correlated motions between particles, which reduces their relative diffusion coefficient, as described in Eq. 15. In our simulation study, inter-HI reduced the association rate by 50%, which was in reasonable agreement with our theoretical prediction. By conducting BD simulations of a simplified model, Antosiewicz and McCammon (18) found that intermolecular HI reduced the rate of enzyme-ligand association by 20%. Frembgen-Kesner and Elcock (19) showed that HI between flexible model proteins also decrease their association rate by ~35−80%.

Our simulation result is also qualitatively consistent with these studies. The effect of inter-HI on assembly is significant. Our theoretical model could qualitatively predict this trend, where the ratio of diffusive-encounter rates of the N-particle object-pairs, in the presence and absence of HI, scales like $N^{2/3}$. This scaling stems from the difference-size dependence of the diffusivities of objects in the presence and absence of HI (see Eqs. 20 and 23), in which $D^{\mathrm{Oseen}} \propto N^{-1/3}$ and $D^{\mathrm{FD}} \propto N^{-1}$. The difference of the ratio of association rates between theoretical and simulation results could be attributed to the size heterogeneity of assembling lipid clusters. For more-accurate predictions, we may need to take into account these effects in the theoretical model.

Hydrodynamic interactions create correlated motions between particles. As expected, in the simulation with inter-HI, long-range correlated motions between lipids in the lipid bilayers were observed, which persist over 40 Å in space and 0.5 μs in time. This is not seen in the simulation without inter-HI. These correlated motions help zip-up lipid clusters in the late stage of membrane self-assembly. Recently, correlated motions between phospholipids in bilayer membranes were observed in a 100-ns atomistic molecular-dynamics simulation with explicit solvent (39). The correlated motions for times ranging from 1 ps to 1 ns were analyzed, giving results that were similar to ours.

For the lipid in a monolayer, the correlation was long-ranged with a decay length of ~25 Å, in good agreement with our CG lipid model in the presence of inter-HI. On the other hand, the correlated motions between lipids in opposing monolayers were weak in the atomistic simulation; this is inconsistent with our results with inter-HI. This discrepancy may be due to use of different lipid models. In our CG model, because each lipid molecule is represented by only two particles, the contact area per molecule between lipids in opposing monolayers is relatively large compared with the atomistic model; this may result in the stronger correlation of the lipid layers. In our simulation, the correlation timescale was ~0.5 μs. Unfortunately, it is difficult to compare our results directly with the atomistic simulations because the simulation timescale in molecular dynamics is too short.

Here, the RPY tensor was adapted to represent HI between lipid molecules, which include all far-field, two-body interactions. A recent simulation study of the association of two nonpolar nanoparticles clearly showed that, at short distances ($<1-2$ nm), molecular-scale effects dominate, giving rise to deviations from continuum hydrodynamic theory (40). Even though a more sophisticated hydrodynamic model was used (41), this deviation from the atomistic simulation results was not eliminated. Therefore, we may need to find a better description of HI at short distances. However, we believe that our simulation results using the RPY tensor still provide the important qualitative features of HI, especially for distances beyond 1−2 nm.

CONCLUSIONS

We have shown that hydrodynamic interactions significantly affect the dynamics of lipid membrane self-assembly. Intermolecular HI reduce the diffusive encounter rate between monomers by 50%. However, the ratio of encounter rate in the presence and absence of HI increases with increasing cluster size. Therefore, in BD simulations without HI, the kinetic parameters of the self-assembly process of a many-particle system will be significantly underestimated. The trend observed in our BD simulation could be qualitatively explained by the simple theory introduced in this study. The effects of HI on self-assembly kinetics can be attributed to the positively correlated motions between lipid molecules that operate over considerable distance- and timescales.

A similar conclusion was reached in our recent BD simulations, which showed that excluded volume effects and HI likely dominate the dynamics of macromolecules in a system mimicking the crowded intracellular environment in *Escherichia coli* (42). Even though the macromolecules do not interact with each other directly via electrostatic and van der Waals energies, HI give rise to similar dynamical correlations between molecules as is observed in this study (42). In these respects, by inducing spatial and temporal correlations, we believe that hydrodynamic interactions likely play an important role in various dynamical processes that take place inside of cells such as signal transduction, polymerization, and chromosome organization. Our future work will explore the role of HI in these processes.

SUPPORTING MATERIAL

Additional analysis, six equations, five figures, and six movies are available at http://www.biophysj.org/biophysj/supplemental/S0006-3495(12)05076-X.

This work was supported in part by grant No. GM-37408 of the Division of General Medical Sciences of the National Institutes of Health.

REFERENCES

1. Karsenti, E. 2008. Self-organization in cell biology: a brief history. *Nat. Rev. Mol. Cell Biol.* 9:255–262.
2. Whitesides, G. M., and B. Grzybowski. 2002. Self-assembly at all scales. *Science.* 295:2418–2421.
3. Dill, K. A., S. B. Ozkan, …, V. A. Voelz. 2007. The protein folding problem: when will it be solved? *Curr. Opin. Struct. Biol.* 17:342–346.
4. Vendruscolo, M., J. Zurdo, …, C. M. Dobson. 2003. Protein folding and misfolding: a paradigm of self-assembly and regulation in complex biological systems. *Philos. Trans. Roy. Soc. A Math. Phys. Eng. Sci.* 361:1205–1222.
5. Alberts, B., A. Johnson, …, P. Walter. 2008. Molecular Biology of the Cell. Garland Science, New York.
6. Drouffe, J. M., A. C. Maggs, and S. Leibler. 1991. Computer simulations of self-assembled membranes. *Science.* 254:1353–1356.
7. Klein, M. L., and W. Shinoda. 2008. Large-scale molecular dynamics simulations of self-assembling systems. *Science.* 321:798–800.
8. Lindorff-Larsen, K., S. Piana, …, D. E. Shaw. 2011. How fast-folding proteins fold. *Science.* 334:517–520.
9. Dror, R. O., A. C. Pan, …, D. E. Shaw. 2011. Pathway and mechanism of drug binding to G-protein-coupled receptors. *Proc. Natl. Acad. Sci. USA.* 108:13118–13123.
10. Kamerlin, S. C. L., S. Vicatos, …, A. Warshel. 2011. Coarse-grained (multiscale) simulations in studies of biophysical and chemical systems. *Annu. Rev. Phys. Chem.* 62:41–64.
11. Tozzini, V. 2005. Coarse-grained models for proteins. *Curr. Opin. Struct. Biol.* 15:144–150.
12. Ermak, D. L., and J. A. McCammon. 1978. Brownian dynamics with hydrodynamic interactions. *J. Chem. Phys.* 69:1352–1360.
13. Ladd, A. J. C. 1993. Short-time motion of colloidal particles: numerical simulation via a fluctuating lattice-Boltzmann equation. *Phys. Rev. Lett.* 70:1339–1342.
14. Malevanets, A., and R. Kapral. 1999. Mesoscopic model for solvent dynamics. *J. Chem. Phys.* 110:8605–8613.
15. Groot, R. D., and P. B. Warren. 1997. Dissipative particle dynamics: bridging the gap between atomistic and mesoscopic simulation. *J. Chem. Phys.* 107:4423–4435.
16. Deutch, J. M., and B. U. Felderhof. 1973. Hydrodynamic effect in diffusion-controlled reaction. *J. Chem. Phys.* 59:1669–1679.
17. Wolynes, P. G., and J. M. Deutch. 1976. Slip boundary-conditions and hydrodynamic effect on diffusion controlled reactions. *J. Chem. Phys.* 65:450–454.
18. Antosiewicz, J., and J. A. McCammon. 1995. Electrostatic and hydrodynamic orientational steering effects in enzyme-substrate association. *Biophys. J.* 69:57–65.
19. Frembgen-Kesner, T., and A. H. Elcock. 2010. Absolute protein-protein association rate constants from flexible, coarse-grained Brownian dynamics simulations: the role of intermolecular hydrodynamic interactions in barnase-barstar association. *Biophys. J.* 99:L75–L77.
20. Baumketner, A., and Y. Hiwatari. 2002. Influence of the hydrodynamic interaction on kinetics and thermodynamics of minimal protein models. *J. Phys. Soc. Jpn.* 71:3069–3079.
21. Cieplak, M., and S. Niewieczerzał. 2009. Hydrodynamic interactions in protein folding. *J. Chem. Phys.* 130:124906.
22. Frembgen-Kesner, T., and A. H. Elcock. 2009. Striking effects of hydrodynamic interactions on the simulated diffusion and folding of proteins. *J. Chem. Theory Comput.* 5:242–256.
23. Kikuchi, N., J. F. Ryder, …, J. M. Yeomans. 2005. Kinetics of the polymer collapse transition: the role of hydrodynamics. *Phys. Rev. E Stat. Nonlin. Soft Matter Phys.* 71:061804.
24. Rotne, J., and S. Prager. 1969. Variational treatment of hydrodynamic interaction in polymers. *J. Chem. Phys.* 50:4831–4837.
25. Yamakawa, H. 1970. Transport properties of polymer chains in dilute solution—hydrodynamic interaction. *J. Chem. Phys.* 53:436–443.
26. Beenakker, C. W. J. 1986. Ewald sum of the Rotne-Prager tensor. *J. Chem. Phys.* 85:1581–1582.
27. Zhou, T., and S. B. Chen. 2006. Computer simulations of diffusion and dynamics of short-chain polyelectrolytes. *J. Chem. Phys.* 124:034904.
28. Cooke, I. R., K. Kremer, and M. Deserno. 2005. Tunable generic model for fluid bilayer membranes. *Phys. Rev. E Stat. Nonlin. Soft Matter Phys.* 72:011506.
29. Dill, K. A., and S. Bromberg. 2003. Molecular Driving Forces: Statistical Thermodynamics in Chemistry and Biology. Garland Science, New York.
30. Doi, M., and S. F. Edwards. 1988. The Theory of Polymer Dynamics. Oxford University Press, Oxford, UK.
31. de Gennes, P. G., and J. Prost. 1993. The Physics of Liquid Crystals. Oxford University Press, Oxford, UK.
32. Northrup, S. H., and J. T. Hynes. 1979. Short-range caging effects for reactions in solution. 1. Reaction-rate constants and short-range caging picture. *J. Chem. Phys.* 71:871–883.
33. von Smoluchowski, M. 1917. Experiments on a mathematical theory of kinetic coagulation of colloid solutions. *Z. Phys. Chem. Stochiom. Verwandtsch. Lehre.* 92:129–168.
34. Kim, S., and S. J. Karrila. 1991. Microhydrodynamics: Principles and Selected Applications. Butterworth-Heinemann, Boston, MA.
35. Rouse, P. E. 1953. A theory of the linear viscoelastic properties of dilute solutions of coiling polymers. *J. Chem. Phys.* 21:1272–1280.
36. Zimm, B. H. 1956. Dynamics of polymer molecules in dilute solution—viscoelasticity, flow birefringence and dielectric loss. *J. Chem. Phys.* 24:269–278.
37. Northrup, S. H., S. A. Allison, and J. A. McCammon. 1984. Brownian dynamics simulation of diffusion-influenced bimolecular reactions. *J. Chem. Phys.* 80:1517–1526.
38. Fahey, P. F., D. E. Koppel, …, W. W. Webb. 1977. Lateral diffusion in planar lipid bilayers. *Science.* 195:305–306.
39. Roark, M., and S. E. Feller. 2009. Molecular dynamics simulation study of correlated motions in phospholipid bilayer membranes. *J. Phys. Chem. B.* 113:13229–13234.
40. Morrone, J. A., J. Li, and B. J. Berne. 2012. Interplay between hydrodynamics and the free energy surface in the assembly of nanoscale hydrophobes. *J. Phys. Chem. B.* 116:378–389.
41. Jeffrey, D. J., and Y. Onishi. 1984. Calculation of the resistance and mobility functions for two unequal rigid spheres in low-Reynolds-number flow. *J. Fluid Mech.* 139:261–290.
42. Ando, T., and J. Skolnick. 2010. Crowding and hydrodynamic interactions likely dominate in vivo macromolecular motion. *Proc. Natl. Acad. Sci. USA.* 107:18457–18462.
43. Humphrey, W., A. Dalke, and K. Schulten. 1996. VMD: visual molecular dynamics. *J. Mol. Graph.* 14:33–38, 27–28.